An evaluation of alternate remote sensing products for forest inventory, monitoring, and mapping of Douglas-fir forests in western Oregon

M.A. Lefsky, W.B. Cohen, and T.A. Spies

Abstract: This research evaluates the utility of several remote sensing data types for the purpose of mapping forest structure and related attributes at a regional scale. Several sensors were evaluated, including (*i*) single date Landsat Thematic Mapper (TM); (*ii*) multitemporal Landsat TM; (*iii*) Airborne Data Acquisition and Registration (ADAR), a sensor with high spatial resolution; (*iv*) Airborne Visible–Infrared Imaging Spectrometer (AVIRIS), a sensor with high spectral resolution; and (*v*) Scanning Lidar Imager Of Canopies By Echo Recovery (SLICER), a lidar sensor that directly measures the height and canopy structure of forest vegetation. To evaluate the ability of each of the sensors to predict stand structure attributes, we assembled a data set consisting of 92 field plots within the Willamette National Forest in the vicinity of the H.J. Andrews Experimental Forest. Stand structure attributes included age, basal area, aboveground biomass, mean diameter at breast height (DBH) of dominant and codominant stems, mean and standard deviation of the DBH of all stems, maximum height, and the density of stems with DBH greater than 100 cm. SLICER performed better than any other remote sensing system in its predictions of forest structural attributes. The performance of the imaging sensors (TM, multitemporal TM, ADAR, and AVIRIS) varied with respect to which forest structural variables were being examined. For one group of variables there was little difference in the ability of the these sensors to predict forest structural attributes. For the remaining variables, we found that multitemporal TM was as or more effective than either ADAR or AVIRIS. These results indicate that multitemporal TM should be investigated as an alternative to either hyperspectral or hyperspatial sensors, which are more expensive and more difficult to process than multitemporal Landsat TM.

Résumé : Ces travaux de recherche avaient pour objectif d'évaluer l'utilité de plusieurs types de données de télédétection à des fins de cartographie de la structure de la forêt et de ses attributs, à une échelle régionale. Plusieurs capteurs ont été évalués, incluant (*i*) Landsat TM à date unique, (*ii*) Landsat TM multi-temporel, (*iii*) ADAR, un capteur à haute résolution spatiale, (*iv*) AVIRIS, un capteur à haute résolution spectrale et (*v*) SLICER, un capteur lidar qui mesure directement la hauteur et la structure du couvert végétal de la forêt. Afin d'évaluer la capacité de chaque capteur à prédire les attributs de la structure du peuplement, un ensemble de données, provenant de 92 parcelles établies dans la Forêt nationale Willamette, à proximité de la Forêt expérimentale H.J. Andrews, ont été recueillies. Les attributs de la structure du peuplement incluaient l'âge, la surface terrière, la biomasse épigée, le diamètre moyen à hauteur de poitrine (dhp) des tiges dominantes et codominantes, la moyenne et l'écart-type du dhp de toutes les tiges, la hauteur maximale et la densité des tiges avec un dhp de plus de 100 cm. La performance du capteur SLICER s'est avérée supérieure à celle de tout autre système de télédétection pour prédire les attributs de la structure de la forêt. La performance des capteurs d'images (TM, TM multi-temporel, ADAR et AVIRIS) variait, selon la variable de la structure de la forêt examinée. Pour un groupe de variables, il y avait peu de différence dans la capacité de ces capteurs à prédire les attributs de la structure de la forêt. Pour les variables restantes, le capteur TM multi-temporel s'est avéré aussi efficace ou supérieur aux capteurs ADAR ou AVIRIS. Ces résultats indiquent que le capteur TM multi-temporel devrait être considéré comme une alternative aux capteurs hyper-spectraux ou hyper-spatiaux, ces derniers étant plus dispendieux et plus difficiles à opérer que le capteur Landsat TM multi-temporel.

[Traduit par la Rédaction]

Introduction

In the last decade, a number of remote sensing devices with advanced capabilities have been introduced. These include hyperspectral and high spatial resolution (hyperspatial) optical sensors, as well as radar and lidar sensors. There have been only a few comparisons of the relative utility of these new and established devices (e.g., Hyppa et al. 1998), and as a result, both remote sensing specialists and users have little information on which to make an informed selec-

Received October 13, 1999. Accepted September 15, 2000. Published on the NRC Research Press website on December 19, 2000.

M.A. Lefsky,[1] W.B. Cohen, and T.A. Spies. USDA Forest Service, Forestry Sciences Laboratory, Pacific Northwest Research Station, Corvallis, OR 97331, U.S.A.

[1]Corresponding author. Present address: USDA Forest Service, Pacific Northwest Research Station, Forestry Sciences Laboratory, 3200 SW Jefferson Way, Corvallis, OR 97331 U.S.A. e-mail: lefsky@fsl.orst.edu

 DOI: 10.1139/cjfr-31-1-78

tion for their purposes. The goal of this study was to provide such a comparison, for the specific purpose of remotely measuring forest structural attributes at a regional scale, for the Douglas-fir – western hemlock (*Pseudotsuga menziesii* (Mirb.) Franco – *Tsuga heterophylla* (Raf.) Sarg.) forest of the Pacific Northwest. Analysis methods were chosen to be applicable at this regional scale. Structural attributes considered include age, basal area, aboveground biomass, mean diameter at breast height (DBH) of dominant and codominant stems, mean and standard deviation of the DBH of all stems, maximum height, and the density of stems with DBH greater than 100 cm.

The most frequently used remote sensing products continue to be from optical sensors that have moderate spatial resolution (10–120 m). Examples include Landsat Thematic Mapper (TM) and Multi-Spectral Sensor (MSS), and SPOT High Resolution Visible (HRV), which are all multispectral sensors with three to six broad spectral bands. In this work, we have used Landsat TM imagery as an example of this group. Optical sensors with two kinds of potential improvements are starting to become generally available. The first are hyperspectral sensors, which expand on the capabilities of sensors like TM by replacing their few broad spectral bands with many narrow spectral bands. The motivation for this modification is the assumption that improved identification of particular spectral features will lead to improved discrimination of cover attributes. This assumption has been supported for the problem of the identification of mineral composition (Van der Meer 1994), and specific features of canopy chemistry (Martin 1994; Zagolski et al. 1996), but not for remote sensing of forest structural attributes. In this work, hyperspectral sensors are represented by images from the Airborne Visible–Infrared Imaging Spectrometer (AVIRIS) airborne remote sensing system (Vane 1987).

The second kind of improvement in sensors is an increase in spatial resolution. Increased spatial resolution allows mapping of features that are smaller than the pixel size of moderate resolution imagery. As a result, it should also allow improved characterization of surface features through the separation of small-scale features, such as canopy foliage, gaps, and shadows that would be mixed in a moderate resolution pixel. More accurate discrimination of these features could result in increased accuracy in forest description. For instance, mature and old-growth conditions might be more accurately discriminated using measurements of the quantity and spatial organization of shadow in their canopies (Cohen and Spies 1992). In this work, high spatial resolution sensors are represented by images from the Airborne Data Acquisition and Registration (ADAR) 5500 airborne sensor (Benkelman et al. 1992).

In addition to the optical remote sensing sensors, two other classes of sensor were considered for inclusion in this study: radar and lidar sensors. Radar sensors are active sensors that generate their own illumination, in this case microwave radiation. The backscatter of the illumination measured by the sensor is proportional to the amount and organization of forest biomass. The backscatter of shorter wavelengths is sensitive to the presence of smaller canopy components, such as foliage and twigs. Larger wavelengths are sensitive to the presence of larger components such as trunks. Despite their early promise, it has been shown that radar sensors are unable to discriminate between forests with more than 250 $Mg \cdot ha^{-1}$ of aboveground biomass (Dobson et al. 1992; Kasischke et al. 1997). In this study, 85% of the study sites (see below) exceed this threshold for aboveground biomass. For this reason, radar sensors were not included in this study.

A second active remote sensor, which we did evaluate in this study, is lidar. The instrument we used, SLICER (Scanning Lidar Imager Of Canopies By Echo Recovery) is one of a new generation of lidar remote sensing systems that augment traditional first-return laser altimetry with a waveform sampling capability (Aldred and Bonnor 1985; Blair et al. 1994; Nilsson 1996). Laser altimeters measure the distance between the sensor and a target through the precise measurement of the time between the emission of a pulse of laser light from the sensor, and the time of detection of light reflected from the target. With this newer class of instruments, the power of the returning laser signal is digitized, resulting in a waveform that records the vertical distribution of the backscatter of laser illumination from all canopy elements (foliar and woody) and the ground reflection, at the wavelength of the transmitted pulse (1064 nm, in the near-infrared). Processing of these waveforms allows us to measure the total height and spatial organization of the canopy; using these measurements we have been able to predict aboveground biomass non-asymptotically to 1200 $Mg \cdot ha^{-1}$ in Douglas-fir – western hemlock forests (Lefsky et al. 1999*b*). Details of the technical aspects of SLICER can be found in Blair et al. (1994) and Harding et al. (1994). Examples of work using SLICER to estimate forest structural attributes can be found in Lefsky et al. (1999*a*, 1999*b*) and Means et al. (1999).

Objectives

Our objective was to evaluate, as directly as possible, the relative ability of five remote sensing data products to predict structural attributes of closed canopy coniferous forests, using methods appropriate for regional-scale mapping. The results of this evaluation will assist us in determining which remote sensing products deserve additional consideration in our ongoing work.

Methods

The evaluation of alternative remote sensing products cannot be separated from the methods used to interpret them, and therefore, no such evaluation can be said to be definitive. In developing this particular comparison, methods were chosen to capture the unique capabilities of each instrument, while remaining logistically practical for our main purpose: mapping forest structure attributes at a regional scale. For the SLICER and TM images, techniques used in previous work (i.e., Cohen and Spies 1992; Lefsky et al. 1999*b*) were adopted without considerable modification. For the AVIRIS image, we used principal component analysis to reduce the dimensionality of the original images so they could be analyzed in a common statistical framework, as in Hyppa et al. (1998). For the ADAR high spatial resolution images, our approach was to use absolute difference filters at a range of resolutions to capture the high-resolution texture of the images. In addition, we used proportional reclassification to capture high resolution image cover information. However, additional techniques could have been applied; for instance, individual tree crown delineation (Gougeon 1995) could have been applied to the ADAR imagery. We did not per-

form such an analysis, because we did not consider it practical for the regional-scale forest-mapping projects that we are concerned with in this work.

Image processing steps

ADAR

Data were collected by the ADAR digital frame camera on September 9, 1992. One hundred and sixty eight individual ADAR scenes were georeferenced to a 10-m SPOT image panchromatic scene and mosaicked. The spatial resolution of the georeferenced image was 1 m. The four spectral bands (blue, green, red, and near infrared) from the ADAR sensor were used as one component of the set of ADAR images to predict stand structural attributes. The spectral bands were also processed using several additional techniques. To create texture images the red spectral band was resampled to resolutions of 2, 4, 8, and 16 m, and an absolute difference filter (Cohen and Spies 1992) was applied. Cohen and Spies (1992) found that the absolute difference filter was successful in relating higher resolution texture information to coarser scale image and forest structure properties. In addition, an existing classification of the ADAR mage was used to create a proportional reclassification (Milne and Cohen 1999). The five classes (shadow, old conifer, young conifer, hardwood, and open) of the existing image were resampled from 1 to 25 m spatial resolution by extracting all the 1-m cover data from within the boundaries of each 25-m pixel. We then computed the proportion of each of the cover classes in the 25-m pixel, resulting in a five-band image, where the value for band one was equal to the proportion of class one in the 25-m pixel, and so on for all the classes. Again, the proportional reclassification image was used to summarize the higher resolution information content so that it could be analyzed at a coarser scale. In the regression analyses we used a data set that included spectral, textural, and proportional reclassification images.

Landsat TM

Six TM spatial mosaics were used for the regression analyses. Each mosaic was created using multiple images collected on each of six dates: March 19, May 6, June 7, July 25, and August 26, 1992; and August 29, 1993. An automated program was used to find ground control points for registration (500+ points in two images), based on image-pattern cross correlation between the TM images and a reference image (R.E. Kennedy and W.B. Cohen, in preparation). Images were then transformed into the tasseled-cap brightness, greenness, and wetness indices (Crist and Cicone 1984; Cohen and Spies 1992). The spatial resolution of the georeferenced images was 25 m. Separate analyses relating each date's image to the forest structural attributes were performed. An image of mean brightness, greenness, and wetness indices was also evaluated. Finally, an image consisting of a layer stack of all six dates (the multitemporal data set) was analyzed. Only the results for the multitemporal and best single month (June) models are presented here.

AVIRIS

AVIRIS images were collected on July 19, 1994. Two images were mosaicked for the regression analyses. Images were corrected for atmospheric effects using the ATREM software package (Gao et al. 1993). Some of the 224 AVIRIS bands contain no usable image data, mostly because of water vapor absorption; these bands were removed. We applied a simple empirical model to remove spatial gradients in brightness due to sun angle and view-angle effects (Kennedy et al. 1997). Images were then registered using the automated GCP identification routine. The spatial resolution of the georeferenced image was 25 m. To simplify analysis, principal component analysis was performed to reduce the large number of spectral bands to 20 principal components, following Hyppa et al. (1998).

Table 1. Average number of plots and selected attribute values by imagery and attribute type.

	No. of observations			Mean		
	Age	Diameter indices	Height	Age	Basal area	Maximum height
ADAR	44	55	50	359	76.3	58
AVIRIS	62	84	75	300	68.1	55
TM	68	92	82	288	66.5	54
SLICER	—	22	22	—	61.1	45

Note: Diameter indices refers to indices calculated from diameter distribution data, such as basal area and biomass.

SLICER

Lidar waveforms were collected by the SLICER instrument in September 1995. SLICER was configured to measure five waveforms cross track, with each waveform covering a footprint 10 m in diameter. Georeferencing of laser footprints was performed by combining laser ranging data with aircraft position, obtained via kinematic global positioning system (GPS) methods, and laser pointing, obtained with a laser-ring gyro inertial navigation system mounted on the SLICER instrument (Blair et al. 1994). Waveforms were processed using both the canopy height profile and the canopy volume profile algorithms, following the procedures in Lefsky (1997) as modified in Lefsky et al. (1999*a*, 1999*b*). As in Lefsky et al. (1999*b*) a variety of canopy indices were used as independent variables: maximum and mean canopy height, canopy cover, variability of the upper canopy surface, and the total volumes of vegetation foliage and empty space within the canopy.

Field measurements of forest stand attributes

To evaluate the ability of each of the four sensors to predict stand structure attributes, we assembled a data set consisting of 92 field plots within the Willamette National Forest in the vicinity of the H.J. Andrews Experimental Forest, near Blue River, Oreg. Field plots were taken from four data sets that are described in Cohen and Spies (1992), Spies and Franklin (1991), Means et al. (1999), and Acker et al. (1998). All plots were in closed-canopy, coniferous forests. Younger forests in this area are dominated by Douglas-fir, while older forests consist of a mix of Douglas-fir and western hemlock. Field data sets had measurements of stem diameters and species collected over either fixed or variably sized plots. Only a portion of the data sets had measurements of stand age and tree height. As a result, the number of plots available for analysis of stand age and height variables is lower than for the other variables. In addition, the spatial extent of the imagery differed, and as a result, the number of plots available to be compared with each image was also variable. The number of plots available for each imagery type and class of variables are presented in Table 1. Table 1 also shows the average age, basal area, and maximum height for plots by imagery type. Calculations of aboveground and foliage biomass were made using equations from the U.S. Fish and Wildlife Service Pacific Northwest Research Station reference stand data base (S. Acker, personal communication). Mean DBH was calculated twice; once for all stems on the plots and once for only the dominant and codominant stems, abbreviated in tables as mean DBH (ALL) and mean DBH (DCD). Mean, standard deviation, minimum, and maximum values for each of the forest structural attributes are given in Table 2, along with the units of each measurement.

Analytical techniques

We chose to predict forest structural attributes as continuous variables, rather than as a set of discrete classes. Experience has shown that this approach offers more flexibility, because the con-

Table 2. Mean, SD, minimum, and maximum values for each of the forest structural attributes in sample plots.

Attribute	Mean	SD	Minimum	Maximum
Age (years)	288.0	186.4	9.0	700.0
Basal area ($m^2 \cdot ha^{-1}$)	70.0	29.4	0.3	146.2
Biomass ($Mg \cdot ha^{-1}$)	681.5	358.1	0.8	1533.0
Mean DBH (ALL) (cm)	34.4	13.2	2.0	66.6
SD of DBH (cm)	30.0	13.6	2.0	60.1
Mean DBH (DCD) (cm)	94.6	18.8	41.0	133.1
Foliage biomass ($Mg \cdot ha^{-1}$)	16.4	6.6	0.1	32.7
Maximum height (m)	54.5	10.3	6.4	106.0
Density of stems >100 cm DBH (no/ha)	36.4	18.1	0.0	82.0

tinuous predictions can be used directly or arranged into multiple sets of classes that match varying purposes (Cohen et al. 2001).

To relate image characteristics to field data, automated methods for extracting data from the images were developed. For the three imaging sensors (TM, ADAR, AVIRIS), a square sampling window was defined on the images, centered at the location of each plot, and this window was used to extract and average pixel data from the image. The sampling window was allowed to vary from between 25 and 475 m in diameter, in 50-m steps, and image data were averaged separately for each sampling window size. The standard deviation of the pixel values in the window were also calculated and used in subsequent analyses. Stepwise multiple regression was then used to relate image characteristics, summarized using each of the sampling window sizes, and forest structural attributes. Of the models generated using the differing sampling window sizes, the model with the maximum adjusted R^2 value was selected to represent that combination of forest structural attribute and imagery type. Field data for the SLICER data set was collected on 50 × 50 m field plots to coincide with 25 SLICER waveforms, and no variable sampling window was used. As with the other data, stepwise multiple regression was used to relate SLICER measured canopy indices to forest structure attributes. One key point in interpreting the results in this paper is that the regression models were not interactively adjusted to optimize the results of any one sensor (i.e., by examining and possibly removing outlier points); uniform methods were used throughout. As a result, individual regressions may have some room for improvement, and the results presented should be viewed in the context of the comparisons of sensors, not as an absolute upper limit to the performance of any one sensor.

Two indices of the quality of each regression equation were used: the coefficient of determination (R^2) and the standard error of the regression. Coefficients of determination indicate the percentage of total variance in the forest structure attributes that is explained by data from each image. All R^2 values reported are adjusted for the effects of multiple independent variables. The standard error of the regressions (SER) is calculated as the standard deviation of the regression's residual values and is an estimate of the distribution of error in the same units as the dependent variable. To compare these values between imagery types, SERs have been presented as a percentage of the mean predicted value for that regression (SER%). As an example, if the value of the standard error of the regression is 20% of the mean predicted value, then 67% of the data points (the percentage of points expected within 1 standard deviation of the mean) have an error less than 20% of the mean value.

Results

For the sake of brevity, we only present results summarizing the ability of each image type to predict each of the forest structural attributes. Table 3 and Fig. 1 present the explanatory power of each imagery type in terms of the adjusted R^2. In every case a statistically significant ($P < 0.05$) relationship was generated, with between 21 and 88% of variance explained. Table 4 and Fig. 2 present the SER as a percentage of the mean predicted value. Regressions resulted in SERs between 15% and 70% of the mean predicted value. SERs are included for reference purposes; while adjusted R^2 and SER are generally well correlated when all analyses are considered, examination of scatterplots indicated that R^2 values were more sensitive to overall goodness of fit.

There was a clear trend in the capacity of each forest structural attributes to be explained by the imagery (Table 5). Forest structural variables were ranked with respect to their relative ability to be predicted by all the imagery types. This was done by ranking the average of the R^2 values associated with the prediction of each forest structural attribute from all imagery types. The best-predicted variables were maximum height and the standard deviation and mean of the DBH of dominant and codominant stems, which is consistent with the findings of Cohen and Spies (1992). One reason for the high ranks of these structural variables is that they are all highly related to the size of the dominant and codominant trees, which are the only trees observed by all but one (SLICER) of the sensors. The next best predicted variables (basal area, foliage biomass, and biomass) integrate the size of all stems in the field plots, not just those of the upper canopy, which may contribute to their lower rankings. The prediction of stand age is complicated by the large number of data points for which we had only categorical data (>450 years, etc.) and the fact that age is not a directly observable attribute. Mean DBH (of all stems) is again probably affected by its reliance on the diameters of all stems, not just those that the sensors can see. The poor prediction of the number of stems greater than 100 cm probably reflects its dependence on a specific aspect of the total diameter distribution, rather than the moments of that distribution.

We also found clear differences among the sensors in their ability to predict forest structure variables (Table 6). Sensors were ranked with respect to their relative ability to predict forest structural attributes. This was done by ranking the average of the R^2 values associated with the prediction of all forest structural attributes from each imagery type. SLICER was overall the top-ranked sensor. Multitemporal TM was the next highest ranked sensor, followed by ADAR and AVIRIS, which were ranked just above the single TM image.

The range of predictability of variables varied by sensor and structural variable. Some forest structure variables, such as maximum height, differ little in the ability of the imaging

Fig. 1. Coefficient of determination (R^2) for prediction of forest structural attributes.

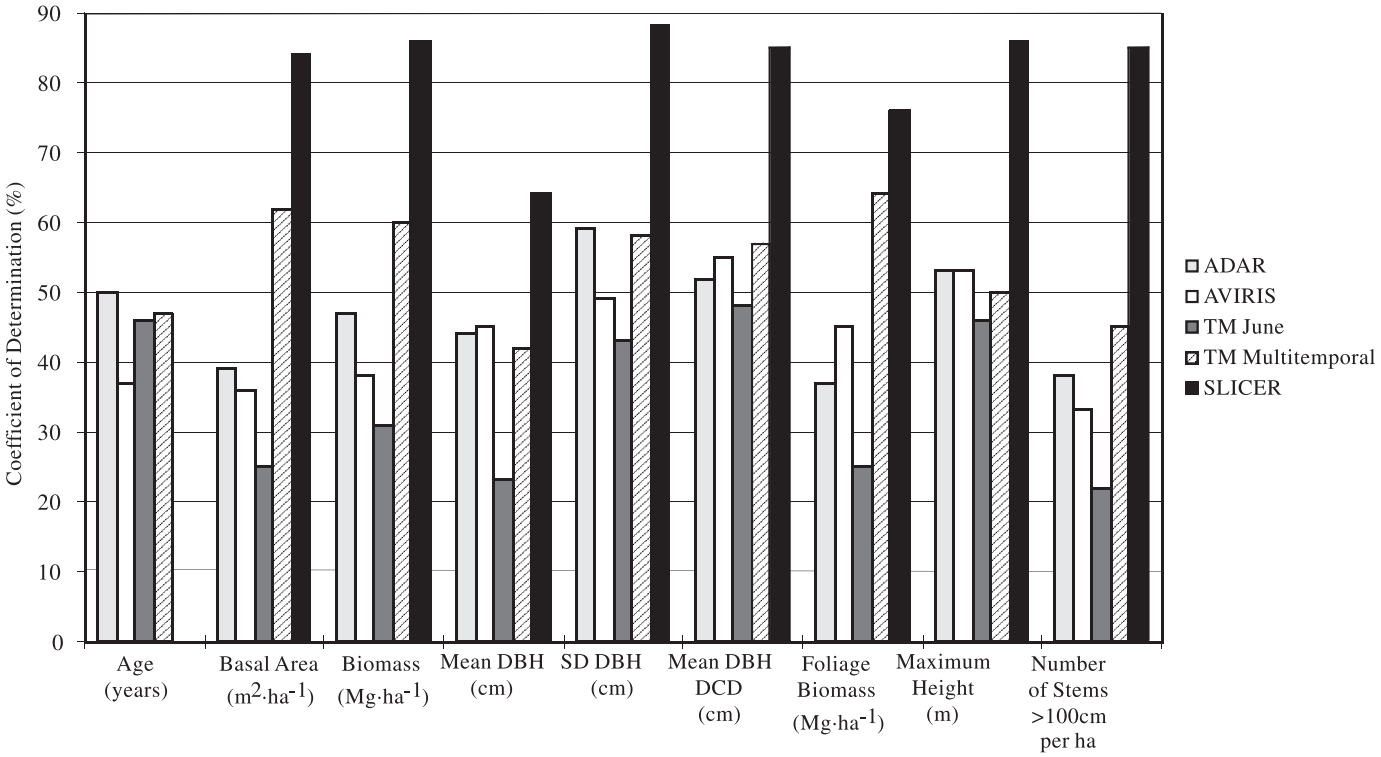

Table 3. Adjusted R^2 (%) values from stepwise multiple regressions relating remotely sensed images and forest stand attributes.

	ADAR	AVIRIS	TM June	TM multitemporal	SLICER
Age	50	37	46	47	—
Basal area	39	36	25	62	84
Biomass	47	38	31	60	86
Mean DBH (ALL)	44	45	23	42	64
SD of DBH	59	49	43	58	88
Mean DBH (DCD stems)	52	55	48	57	85
Maximum height	37	45	25	64	86
Foliage biomass	53	53	46	50	86
Density of stems with DBH >100 cm	38	33	22	45	85
Cost ($/km^2)[a]	75	na	0.13	0.78	300[b]

[a]Cost is for data acquisition only. na, not available.
[b]Cost is for comparable multiple-hit laser altimetry data.

sensors (ADAR, AVIRIS, single-date TM, and multitemporal TM) to predict them (Fig. 1). In contrast, a variable like basal area shows much greater sensitivity to the sensor being used to predict it. These patterns can be summarized into three classes (Table 7) based on performance of the three imaging sensors. We excluded SLICER, because it had much larger R^2 values than the other sensors and because it is likely that only the imaging sensors will be most useful for regional mapping studies in the short term, because of the higher cost and lower availability of lidar devices. The first class of variables is characterized by relatively little difference in the ability of the four imaging remote sensing data sets to predict the variables (e.g., maximum height in Fig. 3). The second class is characterized by a large increase in the ability of multitemporal TM to predict these variables, relative to the three other imaging sensors, and a smaller increase in the ability of ADAR and AVIRIS to predict the variables relative to the single-date TM scene (e.g., basal area in Fig. 3). The third class of variables is characterized by a moderate increase in the ability of multitemporal TM, AVIRIS, and ADAR to predict these forest structural attributes relative to the same ability for the single-date TM scene (e.g., the density of stems greater than 100 cm in DBH in Fig. 3). The distinction between class 2 and class 3 is the relative improvement obtained with the use of multitemporal TM. The R^2 associated with the predictions of variables in class 2 are much higher when made with multitemporal TM relative to those made with AVIRIS or ADAR. The R^2 associated with the predictions of variables in class 3 are similar for all three sensors.

The average relationships observed between the remote sensing products and all of the variables in each of the

Fig. 2. Standard error of regression (SER%) for prediction of forest structural attributes.

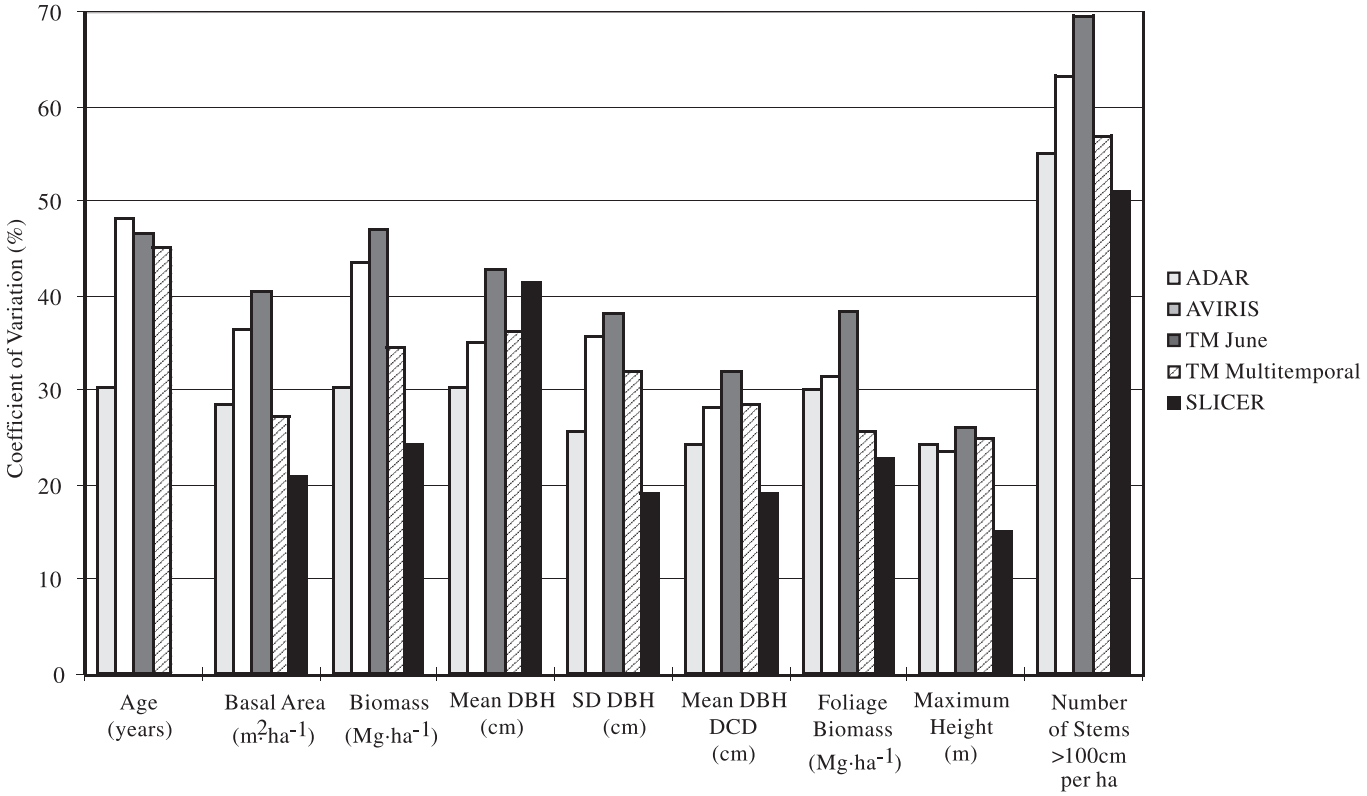

Table 4. Standard error of regressions (SER%) for stepwise multiple regressions relating remotely sensed images and forest stand attributes.

	ADAR	AVIRIS	TM June	TM multitemporal	SLICER
Age	30	48	46	45	—
Basal area	28	37	41	27	21
Biomass	30	44	47	35	24
Mean DBH (ALL)	30	35	43	36	41
SD of DBH	26	36	38	32	19
Mean DBH (DCD)	24	28	32	28	19
Maximum height	30	31	38	26	23
Foliage biomass	24	24	26	25	15
Density of stems with DBH >100 cm	55	63	70	57	51

Note: Standard error of the regressions is given as a percentage of the mean predicted value.

classes (Fig. 4) are the same as those described for the individual forest structural attributes illustrated in Fig. 3. There is little difference in the ability of the four imaging sensors to predict forest structural attributes in class 1. Predictions of forest structural attributes in class 2 from the multitemporal TM image were higher than those made from either AVIRIS or ADAR, which were in turn higher than those made from the single TM image. ADAR, AVIRIS, and multitemporal images all showed an increased ability to predict the forest structural attributes in class 3 (relative to the ability of single-date TM), but no one of these sensors performed considerably better than the others.

Discussion

This study found that the lidar remote sensing data performed better than other remote sensing systems in its predictions of forest structural attributes. This conclusion had been suggested before by comparison of results obtained with lidar (Lefsky et al. 1999*a*, 1999*b*; Means et al. 1999) to unrelated studies that predict similar forest structural attributes using radar and optical sensors. However, the small number of field plots (22) available to use in the SLICER analysis, and the lower mean values of key structural attributes in those field plots (Table 1), prevents an unequivocal assertion of the relative ability of SLICER and the other sensors. This concern can be partially addressed by comparison of field measured heights to field measured forest stand attributes. The most important variable used in the SLICER prediction of aboveground biomass is the mean height of the lidar waveforms. In this study, the mean height of the waveforms has been shown to be very highly correlated with the

Table 5. Relative success of predictions of each forest structural variable for all remote sensing types ranked by R^2 (%).

Variable	SER%	R^2 (%)
Maximum height	26	59
SD of DBH	30	59
Mean DBH (DCD)	23	58
Basal area	36	52
Foliage biomass	30	49
Biomass	31	49
Age	42	45
No. of stems >100 cm	59	45
Mean DBH (ALL)	37	44

Table 6. Relative success of sensors at predicting forest structural variables, ranked by R^2 (%).

Sensor	SER%	Adjusted R^2 (%)
SLICER	27	82
TM multitemporal	35	54
ADAR	31	47
AVIRIS	38	43
TM June	42	34

Table 7. Forest structural variables by class.

Class 1	Class 2	Class 3
Age	Basal area	Mean DBH (ALL)
Mean DBH (DCD)	Biomass	Stems >100 cm
Maximum height	Foliage biomass	
SD of DBH		

Note: See text for explanation of classes.

mean height of dominant and codominant trees in each plot (R^2 = 85%). Given this high correlation, we can, for our purposes, consider the SLICER height measurements as nearly identical to field height measurements and can use field measurements of height as a surrogate for SLICER measurements. In the field plot data set from this study we have 72 plots with both biomass and field-measured mean height (of the dominant and codominant stems) measurements, and the correlation between these two variables is 78%, as compared with the 86% correlation between SLICER measured mean height and biomass in the 22 SLICER plots used in this study. Preliminary work on a larger (75 plot) data set of field plots has determined that SLICER is still capable of explaining >85% of the variance in aboveground biomass. While these analyses are not definitive, it does suggest that the ability of SLICER to predict forest structural attributes is likely to remain high even when larger data sets are considered. Hyppa et al. (1998), in a study directly comparing a radar altimeter (HUTSCAT) to a variety of other sensors, concluded that the radar altimeter was superior for the prediction of variables such as stand volume and basal area. In that study, the sample size of all data sets was equal.

While lidar remote sensing has many advantages over the other sensors considered here, it is not, by itself, practical for large operational remote sensing projects at this time.

Fig. 3. R^2 (%) values for predictions of forest structural variables that are typical of the three classes of response observed in the data, from each of the four imagery types.

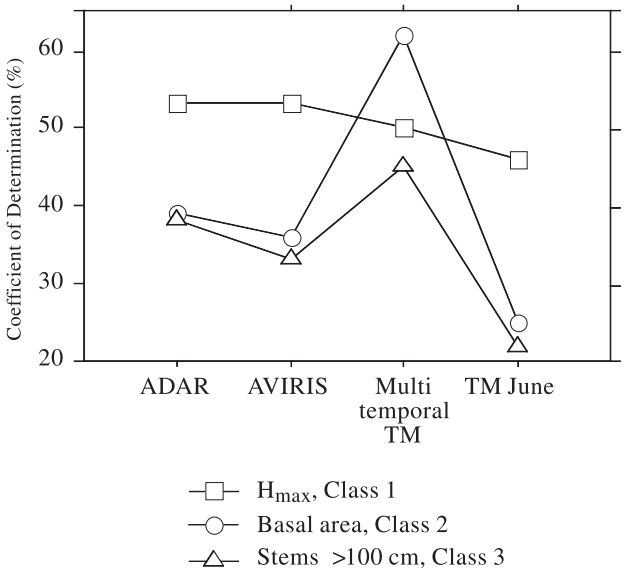

Fig. 4. Average R^2 values for predictions of variables in each of the three classes of response, from each of the four imagery types. Error bars are SE. See text for definition of classes.

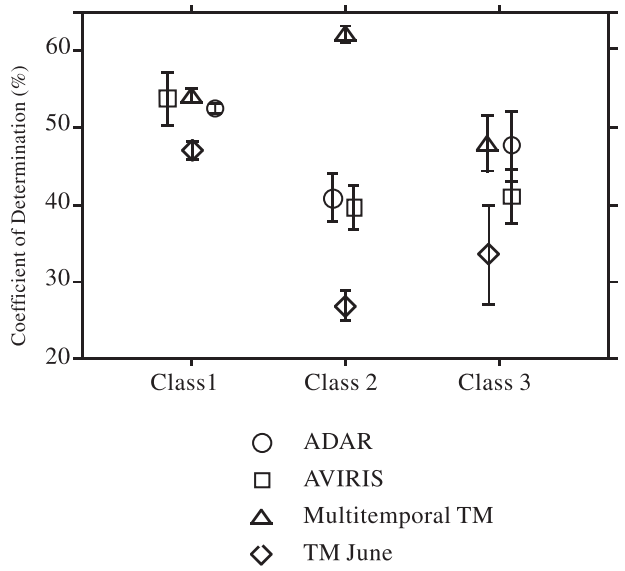

This is due to its high cost (approximately \$300/km^2) and the fact that sensors capable of making lidar measurements over large areas are only starting to come into use. Nevertheless, lidar is likely to play an increasingly large role in regional scale remote sensing projects, as global data from the VCL (vegetation canopy lidar; Dubayah et al. 1997) mission become available. Although VCL data will be available for only a sample of the earth's surface (approximately 5%), it has the potential to increase the accuracy of predictions of forest structural attributes made with other remote sensing systems through sensor fusion. In practice, one way that sensor fusion can be accomplished is to replace or augment field data with the data from the VCL sensor. Because we

Table 8. R^2 (%) and SER% for models predicting basal area from one, two, and six TM Images.

	Adjusted R^2 (%)	SER%
Single date (June)	25	41
Two dates (March, July)	50	32
Multitemporal (all six dates)	62	27

will have a large volume of data from VCL, relative to the amount we would normally have from field sites, we can use this data to better characterize local variations in the relationship between image characteristics and forest structural attributes.

The results of this study suggest that the selection of an optimal imaging remote sensing data sets (i.e., ADAR, AVIRIS, TM) for regional-scale mapping is strongly dependent on the forest structural attribute of interest. For the forest structural attributes such as age, mean DBH (dominant and codominant stems), maximum height, and the standard deviation of DBH, we saw little difference in the predictions made by the imaging sensors. Within this context, Landsat TM has a clear advantage over the other sensors in terms of cost, storage requirements, spatial availability, and the existence of a substantial literature of methods for geometric rectification, radiometric correction, and analysis for extracting forest structural attributes. Furthermore, the advantages of this sensor have increased with the launch of Landsat 7, which carries the enhanced thematic mapper + sensor (see below).

For the forest structural attributes such as basal area, biomass, and foliage biomass, substantial increases in predictive power were obtained using the multitemporal Landsat TM data set in comparison with the other imaging sensors. Both ADAR and AVIRIS showed more modest improvements over single-date TM. We believe that multitemporal TM represents the best approach for measuring these attributes, primarily for the same reason that TM is a sensor of choice for other attributes (cost, storage requirements, spatial availability, and availability of literature). While multitemporal data will cost more and have larger storage requirements than single-data TM, this is mitigated for two reasons. First, now that Landsat 7 has been launched, the distribution of TM is being handled by the EROS data center, not by a private firm, and its cost is set at the cost of distribution, currently about $600 per scene. With the price of TM falling by over 80%, spatially extensive multitemporal data sets will be correspondingly more affordable. Secondly, whereas we used six TM scenes in the multitemporal data set for this study, follow-up analysis suggests that substantial improvements in predictive power can be achieved with only two scenes. Table 8 and Fig. 5 document the results of this analysis for one of the variables in class 2, basal area. As illustrated in the figures and quantified in the table, the majority of the improvement in predictive power occurs with the addition of the second image. March and July were selected as the optimal months for the 2-month analysis by analyzing all possible combinations of dates. That these two dates achieve the best results is probably due to the combination of low and high sun angles obtained in these two images, which allows more precise estimation of the degree of shadowing in the canopy, which is closely related to the height and variability of the canopy. As a consequence of moving from a six-date analysis to a two-date analysis, the cost of the multitemporal analysis is reduced by a factor of three.

Fig. 5. Prediction of basal area from single-date (June) TM (R^2 = 25%), two dates (March, July) of TM (R^2 = 50%), and six dates of TM (R^2 = 62%). See text for dates of surveys.

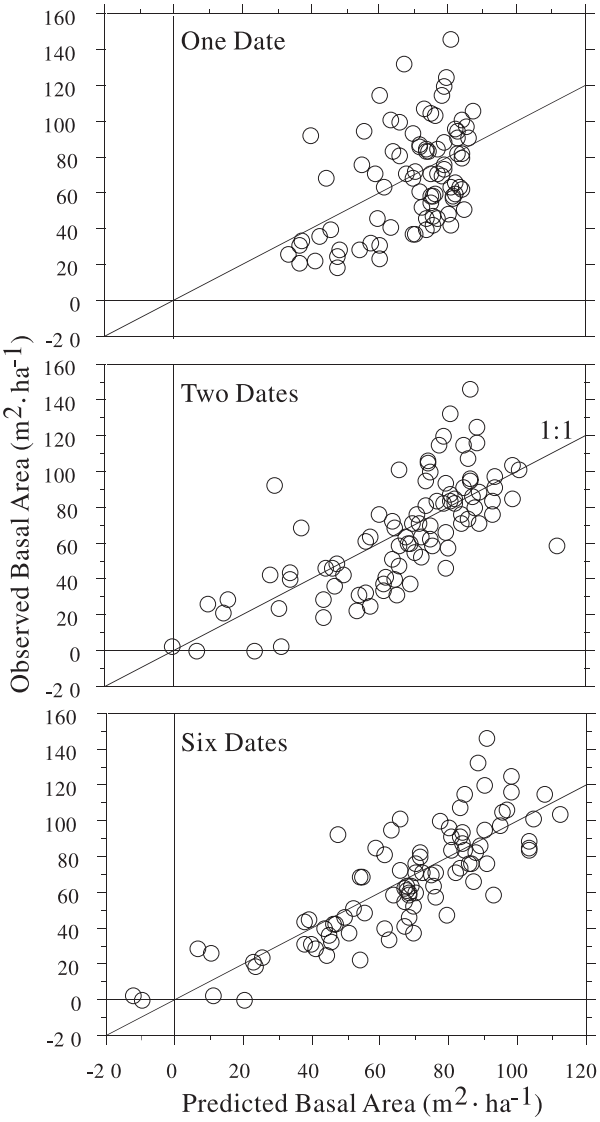

ADAR, AVIRIS, and multitemporal TM all showed a moderate level of improvement for the prediction of the forest stand attributes in class 3 (Mean DBH of all stems, and the density of stems >100 cm in DBH), relative to the single-date TM. However, there was no clear difference between the performance of these three sensors (Fig. 4), so for the reasons of cost and efficiency cited above, multitemporal analysis of TM is preferable over ADAR or AVIRIS.

Conclusions

Lidar appears to offer substantial improvements over the other sensors considered in the accuracy of its predictions of forest structural attributes. The availability, spatial coverage,

and cost of this data will limit its immediate applicability; however, data from NASA's VCL sensor has the potential to increase the accuracy of predictions of forest structural attributes through sensor fusion with data from imaging sensors. Single-date Landsat TM is comparable with ADAR, AVIRIS, and multitemporal TM in its ability predict forest structural attributes such as stand age, mean DBH of dominant and codominant stems, maximum height, and the standard deviation of DBH. For these attributes, the continued use of TM is recommended. Multitemporal TM is superior to ADAR, AVIRIS, and single-date TM is its ability to predict forest structural attributes like basal area, biomass, and foliage biomass. While the results in this report were obtained using a six-date multitemporal image, substantial increases in the quality of predictions of basal area were found when using only two images over single-date TM. We recommend that research on the use of multitemporal images be considered for this class of attributes. ADAR and AVIRIS, which incorporate (respectively) high spatial resolution and hyperspectral capabilities, did not appear to be consistently superior for any set of forest structural attributes. These two sensors did offer some improvement in the quality of predictions over single-date TM for some of the forest structural attributes. However, the limited spatial distribution and availability, high cost, and relatively complex processing requirements of these data sets indicate that multitemporal TM should be investigated before either of them.

Acknowledgements

The work was perfomed at the USDA Forest Service Pacific Northwest Research Station and was supported by a grant from the USDI Fish and Wildlife Service to Drs. Spies and Cohen.

References

Acker, S.A., McKee, W.A., Harmon, M.E., and Franklin, J.F. 1998. Long-term research on forest dynamics in the Pacific Northwest: a network of permanent forest plots. *In* Forest biodiversity in North, Central, and South America and the Carribean: research and monitoring. *Edited by* F. Dallmeier, and J.A. Comiskey. Parthenon Publishing Group, Inc., New York. pp. 93–106.

Aldred, A.H., and Bonnor., G.M. 1985. Applications of airborne lasers to forest surveys. Can. For. Serv. Petawawa Natl. For. Inst. Inf. Rep. PI-X-51.

Benkelman, C.D., Verbyla, D., and Cohen, W.B. 1992. Application of high resolution digital imagery to forestry studies. *In* Proceedings of the American Society for Photogrammetry and Remote Sensing Annual Meeting, 29 Feb. – 5 Mar. 1992, Albuquerque, N.M. American Society for Photogrammetry and Remote Sensing, Washington D.C. pp. 28–35.

Blair, J.B., Coyle, D.B., Bufton, J.L., and Harding, D.J. 1994. Optimization of an airborne laser altimeter for remote sensing of vegetation and tree canopies. *In* Proceedings of IEEE Geosciences and Remote Sensing Society, 8–12 Aug. 1994, Pasadena, Calif. Institute of Electrical and Electronics Engineers, Piscataway, N.J. Vol. II. pp. 939–941.

Cohen, W.B., and Spies, T.A. 1992. Estimating structural attributes of Douglas-fir/western hemlock forest stands from Landsat and SPOT imagery. Remote Sens. Environ. **41**: 1–17.

Cohen, W.B., Maiersperger, T.K., Spies, T.A., and Oetter, D.R. 2001. Modeling forest cover attributes as continuous variables in a regional context with thematic mapper data. Int. J. Remote Sens. In press.

Crist, E.P., and Cicone, R.C. 1984. A physically-based transformation of thematic mapper data—the TM tasseled cap. IEEE Trans. Geosci. Remote, 22: 256–263.

Dobson, M.C., Ulaby, F.T., Letoan, T., Beaudoin, A., Kasischke, E.S., and Christensen, N.L. 1992. Dependence of radar backscatter on coniferous forest biomass. IEEE Trans. Geosci. Remote, **29**: 444–450

Dubayah, R., Blair, J.B., Bufton, J.L., Clark, D.B., JaJa, J., Knox, R., Luthcke, S.B., Prince, S., and Weishample, J. 1997. The vegetation canopy lidar mission. *In* Land satellite information in the next decade II: sources and applications. American Society for Photogrammetry and Remote Sensing, Washington D.C. pp. 100–112.

Gao, B.C., Hedebrecht, K., and Goetz, A.F.H. 1993. Derivation of scaled surface reflectances from AVIRIS data. Remote Sens. Environ. **44**: 165–178.

Gougeon, F.A. 1995. A crown-following approach to the automatic delineation of individual tree crowns in high spatial resolution aerial images. Can. J. Remote Sens. **21**: 274.

Harding, D.J., Blair, J.B., Garvin, J.G., and Lawrence, W.T. 1994. Laser altimeter waveform measurement of vegetation canopy structure. *In* Proceedings of IEEE Geosciences and Remote Sensing Society, 8–12 Aug. 1994, Pasadena, Calif. Institute of Electrical and Electronics Engineers, Piscataway, N.J. Vol II. pp. 1251–1253.

Hyppa, J., Huuppa, H., Inkinen, M., and Engdahl, M. 1998. Verification of the potential of various remote sensing data sources for forest inventory. *In* Proceedings of IEEE Geosciences and Remote Sensing Society, 6–10 July 1998, Seattle, Wash. Institute of Electrical and Electronics Engineers, Piscataway, N.J. pp. 1812–1814

Kasischke, E.S., Melack, J.M., and Dobson, M.C. 1997. The use of imaging radar for ecological applications—a review. Remote Sens. Environ. **59**: 141–156.

Kennedy, R.E., Cohen, W.B., and Takao, G. 1997. Empirical methods to compensate for a view-angle-dependent brightness gradient in AVIRIS Imagery. Remote Sens. Environ. **62**: 277–291.

Lefsky, M.A. 1997. Application of lidar remote sensing to the estimation of forest canopy and stand structure Ph.D. dissertation, Department of Environmental Science, University of Virginia, Charlottesville.

Lefsky, M.A., Harding, D., Cohen, W.B., and Parker, G.G. 1999*a*. Surface lidar remote sensing of basal area and biomass in deciduous forests of eastern Maryland, USA. Remote Sens. Environ. **67**: 83–98.

Lefsky, M.A., Cohen, W.B., Acker, S.A., Spies, T.A., Parker, G.G., and Harding, D. 1999*b*. Lidar remote sensing of biophysical properties and canopy structure of forest of Douglas-fir and western hemlock. Remote Sens. Environ. **70**: 339–361.

Martin, M.E. 1994. Measurements of foliar chemistry using laboratory and airborne high spectral resolution visible and infrared data. Ph.D. dissertation, University of New Hampshire, Durham.

Means, J.E., Acker, S.A., Harding, D.A., Blair, B.J, Lefsky, M.A., Cohen, W.B., Harmon, M., and McKee, W.A. 1999. Use of large-footprint scanning airborne lidar to estimate forest stand characteristics in the western Cascades of Oregon. Remote Sens. Environ **67**: 298–308.

Milne, B.T., and Cohen, W.B. 1999. Multiscale assessment of binary and continuous land cover variables for MODIS validation,

mapping, and modeling applications. Remote Sens. Environ. **70**: 82–98.

Nilsson, M. 1996. Estimation of tree heights and stand volume using an airborne lidar system. Remote Sens. Environ. **56**: 1–7.

Spies, T.A., and Franklin, J.F. 1991. The structure of natural young, mature, and old-growth Douglas-fir forests in Oregon and Washington. *In* Wildlife and vegetation of unmanaged Douglas-fir forests. *Edited by* L.F. Ruggiero, K.B. Aubry, A.B. Carey, and M.H. Huff. USDA Forest Service, Pacific Northwest Research Station, Portland, Oreg. pp. 91–109.

Van der Meer, F. 1994. Extraction of mineral absorption features from high-spectral resolution data using non-parametric geostatistical techniques. Int. J. Remote Sens. **15**: 2193–2214.

Vane, G. (*Editor*). 1987. Airborne visible/ infrared imaging spectrometer (AVIRIS). Jet Propulsion Laboratory, National Aeronautics and Space Administration, Pasadena, Calif. JPL Publ. 87-38.

Zagolski, F.P.V., Romier, J., Alcayde, D., Fontanari, J., Gastellu-Etchegorry, J., Giordano, G., Marty, G., Mougin, E., and Joffre, R. 1996. Forest canopy chemistry with high spectral resolution remote sensing. Int. J. Remote Sens. **17**: 1107–1128.